Fouling is the beginning: Upcycling biopolymer-fouled substrates for fabricating high-permeance thin-film composite polyamide membranes

Ruobin Dai,[a] Hongyi Han,[a] Tianlin Wang,[a] Jiayi Li,[a] Chuyang Y. Tang,[b] and Zhiwei Wang*[a]

[a] State Key Laboratory of Pollution Control and Resource Reuse, Shanghai Institute of Pollution Control and Ecological Security, School of Environmental Science and Engineering, Tongji University, Shanghai 200092, China.

[b] Department of Civil Engineering, The University of Hong Kong, Pokfulam Road, Hong Kong S.A.R., China.

* To whom all correspondence should be addressed.

Tel.: +86-21-65975669, Fax: +86-21-65980400, E-mail address: zwwang@tongji.edu.cn

Revised Manuscript (2nd) Submitted to Green Chemistry (Dec, 2020, Marked version)

Abstract

The recycling of end-of-life water purification membranes is of great significance for environmental sustainability. However, only techniques for downcycling end-of-life high-pressure membranes are available. Here, we propose to upcycle fouled microfiltration membranes for fabricating new high-pressure polyamide (PA) thin-film composite membranes via interfacial polymerization (IP). A cross-linked, defect-free, and ultrathin PA active layer was formed on biopolymer-fouled substrates. In contrast to the decreased pure water permeance of substrates caused by biopolymer fouling, the upcycled membranes show excellent water permeance (~30 L m^{-2} h^{-1} bar^{-1}) and Na_2SO_4 rejection (~95%) in nanofiltration tests for water purification. The biopolymer foulants regulate the IP process and the formation of the PA layer. Furthermore, the foulants between the PA layer and substrate can create additional channels for water transport. The PA layer formation could also be achieved on real fouled microfiltration substrates. This proof-of-concept study paves the way for upcycling fouled/end-of-life low-pressure membranes to fabricate new high-pressure membranes for water purification, forming a closed eco-loop of membrane recycling.

Keywords: Membrane upcycling; closed loop; interfacial polymeriaztion; end-of-life membrane; polyamide.

1. Introduction

Synthetic membranes, largely made of polymers [1], are widely used in various industries, such as water purification [2,3], bioprocessing [4], and food processing [5]. Membrane separation is favored over other processes in many applications, due to its energy efficiency, simplicity, manufacturing scalability and small footprint [1]. However, commercial polymeric membranes are generally recognized to have low sustainability as membranes need to be replaced and abandoned after reaching the end of their life [6,7], mainly resulting from irreversible membrane fouling [8,9]. By 2020, the global market for membrane components is estimated to reach $20 billion[10], while nearly 30,000 tons of plastic waste will be correspondingly discarded in landfills every year worldwide [11]. With the increasing popularity of membranes in global industries (with an annual growth rate of 10.5%)[10], the severely negative environmental impacts of the disposal of fouled/end-of-life membranes should be addressed. Sustainable fabrication approaches for membrane and support materials have been developed in recent years[12–16]. However, the recycle of the membranes to go after reaching end-of-life still remains a critical issue. Environmental engineers and material scientists have attempted downcycling end-of-life high pressure reverse osmosis/nanofiltration (RO/NF) membranes into NF/ultrafiltration (UF) membranes after appropriate treatment.[17,18] Nevertheless, for fouled/end-of-life low pressure membranes (MF/UF), how to recycle these membranes in an environmentally friendly and technically feasible way remains a great challenge.

For fouled/end-of-life membranes, biopolymers are one of the most important foulants.[19,20] Biopolymers such as polysaccharides, proteins, and humic acids cause fouling during the treatment of surface water by MF/UF processes.[21,22] Microbial extracellular polymeric substances (EPS) are the major contributor to membrane fouling in engineered membrane bioreactors.[23,24] In membrane separation of bioprocessing or food processing, those biopolymers, being the target products in the feed liquid, are also responsible for membrane

fouling [25,26].In these typical scenarios, the biopolymers are thought to be unfavorable foulants causing a loss of permeance or inducing the end of life of a membrane. However, biopolymers are often also raw materials or natural modifiers used to fabricate environmentally friendly membranes.[27–30] Accordingly, can we utilize biopolymer foulants on a membrane surface (or in pores) as a possible novel biomaterial platform to further fabricate NF/RO membranes?

The gold standard for fabricating commercial RO and NF membranes is forming a polyamide (PA) layer on a porous substrate via interfacial polymerization (IP) and constructing a thin-film composite (TFC) structure.[31–33] Interestingly, recent studies have progressively highlighted the prospect of modifying substrates to fabricate high-performance TFC membranes.[34,35] The reported coatings on substrates (*e.g.*, tannic acid-Fe^{3+} complexes[36], polydopamine[37], carbon nanotubes[38,39], and graphene oxide[40,41]) have been proven effective for improving the quality of the PA layer and the separation performance of the TFC membranes. Inspired by this, we postulate that a biopolymer fouled MF/UF membrane can be a possible substrate for fabricating high-permeance NF/RO membranes.

Herein, for the first time, we upcycled various biopolymer-fouled MF substrates to directly fabricate TFC PA membranes via IP. The as-prepared TFC membranes on the biopolymer-fouled substrate showed a higher rejection rate and greater membrane water permeance compared to that on the control substrate. The mechanisms of biopolymer-fouled substrate-based PA membranes in enhancing NF performance were further elucidated. The feasibility of the upcycling strategy was evaluated on the real fouled MF substrates. This proof-of-concept study will pave the way for forming a closed eco-loop of membrane material recycling.

2. Experimental section

2.1 Materials and chemicals

Commercially available polyether sulfone (PES) MF membranes with a pore size of 0.22 μm as substrates were supplied by YiBo Co., Ltd. (China). The PES membranes were directly used without any pretreatment. All working solutions were prepared using Milli-Q water throughout the study, unless otherwise stated. Sodium alginate (SA) as the model polysaccharide foulant was purchased from Aladdin Chemical Co. Ltd. (China), while bovine serum albumin (BSA) as the model protein foulant and humic acid (HA) were obtained from Sigma-Aldrich (Figure S1). Piperazine (PIP, 99%), trimesoyl chloride (TMC, 98%), and *n*-hexane (≥98%) from Aladdin were used for interfacial polymerization to form the PA selective layer. Inorganic salts (NaCl, $MgCl_2$, $CaCl_2$, $MgSO_4$ and Na_2SO_4) and DMF for PES dissolution were also supplied by Aladdin. Citrate-stabilized GNP solution (average particle size of 5 nm) was purchased from BBI Solutions (UK). All chemicals were used as received.

2.2 Preparation of biopolymer fouled substrates

Microbial EPS was extracted from activated sludge collected from a municipal wastewater treatment plant (Figure S2). Each model biopolymer solution was prepared by dissolving 10 mg/L SA, BSA, HA and EPS in Milli-Q water, respectively. PES MF membranes (12.56 cm^2) were fouled by vacuum filtration of 80 mL solution of each model biopolymer foulant at 0.02 MPa vacuum pressure (Figure 1A), followed by compaction using 100 mL water. For example, the SA fouled PES microfiltration membrane was fouled by solution of SA and denoted as SA-F (Table S1). The resulting density of each foulant on the PES MF membrane was measured by the total organic carbon (TOC) of the feed and permeate. The composition of EPS in the permeate was also determined by the anthrone method and modified Lowry method for the corresponding permeate.[42]

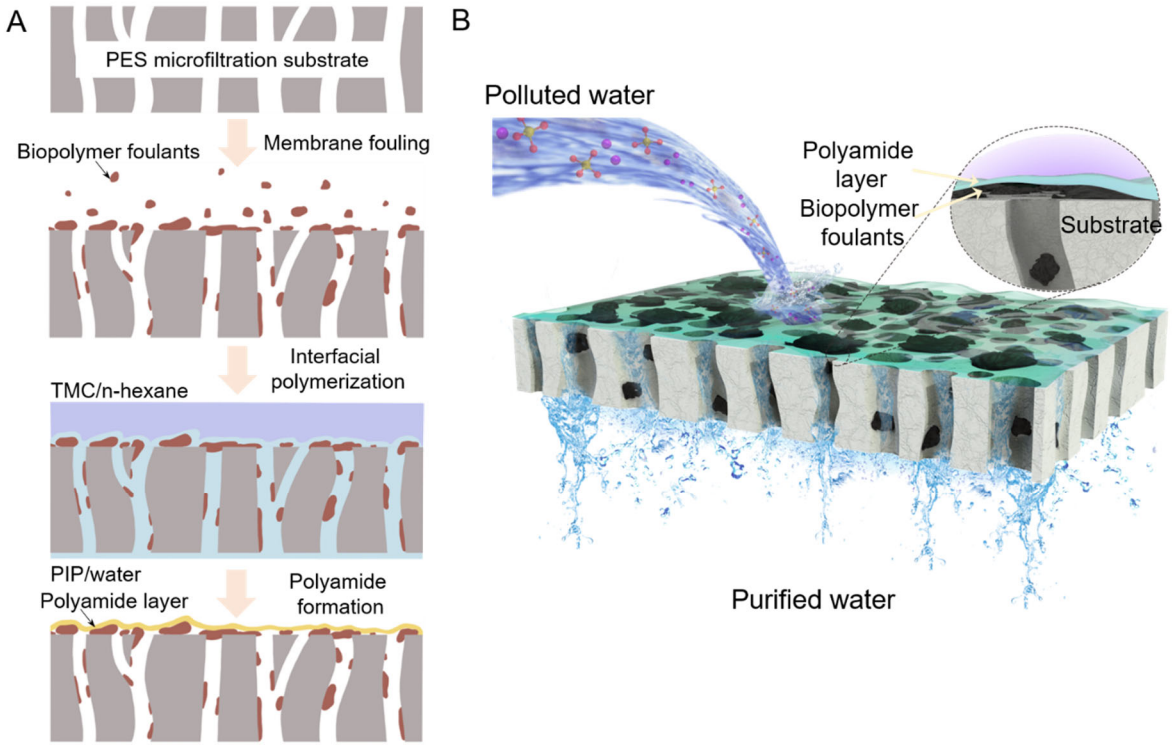

Figure 1. (A) Schematic illustrating TFC PA membrane fabrication on a biopolymer-fouled substrate via interfacial polymerization; (B) Schematic of water purification using the upcycled TFC PA membrane.

2.3 Fabrication of PA membrane on fouled PES substrates

The fabrication process of TFC PA membranes on fouled or control PES substrates is illustrated in Figure 1A. TFC NF membranes were fabricated by forming a PA selective layer on top of the control or fouled PES membrane via IP. The control or fouled PES substrates were first framed and immersed in 0.05 wt/v % PIP aqueous solution for 2 min. After removal of excess PIP/water solution, the surface of the substrate was exposed to 0.04 wt/v % TMC in hexane for a 30 s IP reaction. After removing the excess TMC solution, the membranes were vertically dried for 1 min, washed with *n*-hexane and then oven-cured at 60°C for 5 min to obtain TFC PA membranes. The resulting membranes were stored in water at 4°C for further use. The

abbreviations of as-fabricated TFC PA membranes upcycled from biopolymer fouled substrates can be found in Table S1.

2.4 PA layer formation on real fouled MF substrates

Real fouled MF membranes (TP7 in Figure S3, Shanghai Zizheng Environmental Technology Co., Ltd.), which were used as substrates for PA layer formation, were obtained from a large-scale membrane bioreactor in Langxia municipal wastewater treatment plant, Shanghai, China. The membranes were used for the treatment of municipal wastewater for nearly 4 years and exposed to several cleaning cycles during the operation. Before exposure to IP, the membranes were gently scoured by water and cut into membrane disks with diameters of 50 mm. The IP process on the real fouled substrates was nearly the same as those on artificially fouled substrates, except that three monomer concentrations (*i.e.*, 0.05 wt/v%, 0.20 wt/v% and 0.40 wt/v% for PIP/water; 0.04 wt/v%, 0.16 wt/v% and 0.32 wt/v% for TMC/*n*-hexane, respectively, named as NF-real-hexane-1, -2 and -3) were applied. To modify the strategy based on green chemistry perspective, additional tests were conducted using *n*-heptane to replace *n*-hexane solvent while each monomer concentration for PA membrane fabrication was unchanged (corresponding to NF-real-heptane-1, -2 and -3, respectively).

2.5 In-situ preparation of upcycled TFC PA membranes in a cross-flow cell

The in-situ preparation of upcycled TFC PA membranes was conducted in a cross-flow cell (Figure 2) throughout the whole fouling and IP process, during which only pipeline connection was changed. The PES substrate with an effective area of 50 cm^2 was fouled by 10 mg/L EPS in the experimental cross-flow set-up as illustrated in Figures 2A, B, until the water flux reached the value equal to that of the EPS-F. The cross-flow cell containing fouled substrate was then removed from the experimental set-up. The clean or cross-flow fouled PES substrates were exposed to 0.05 wt/v% PIP/water (20 mL) for 2 min (Step 1 in Figure 2C). After removal of excess PIP/water solution by nitrogen flushing (Step 2), the surface of the substrate was then

exposed to 0.04 wt/v% TMC/hexane (20 mL) for a 30 s IP reaction (Step 3). The excess TMC solution was then removed by flushing of nitrogen gas again (Step 4). The membranes were washed with 40 mL (8 L/m^2) *n*-hexane (Step 5) and then treated by 20 mL (4 L/m^2) 60°C hot water for 5 min (Step 6) to obtain *in-situ* formed TFC PA membranes. The resulting membranes were stored in water at 4°C for further use.

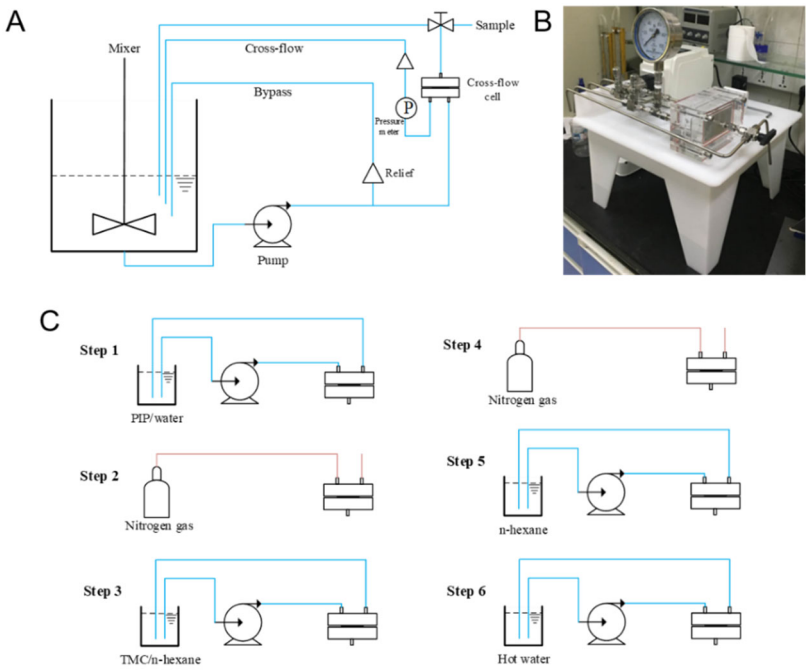

Figure 2. (A) Illustration and (B) photo of laboratory cross-flow filtration setup used for membrane fouling; (C) Illustration of the in-situ formation process of upcycled TFC PA membranes. Note that the substrate/membrane was fixed in the cross-flow cell throughout the whole fouling and in-situ IP process, during which only pipeline connection was changed.

2.6 Membrane characterization

SEM images were taken with a Hitachi S-4800 field emission scanning electron microscope (FESEM) at 5.0 kV. The pore size distribution on the surface of the substrates was evaluated by analyzing the SEM images using Nano Measurer software. At least six SEM images (50-100 counts for each SEM image) from three individual samples were analyzed to obtain the

pore size distribution and the average value. The water contact angle of the membrane surface was determined through sessile drop contact angle measurements at room temperature (OCA 15 Plus, Data Physics GmbH, Germany). At least eight random locations were measured for each membrane coupon. The PIP uptake by clean or fouled substrates was measured using the weight change after immersion in an aqueous solution of 0.05 wt/v % PIP for 2 min.

AFM (Veeco NanoScope MultiMode III) was used to analyze the membrane surface roughness in peak force tapping mode, as well as the thickness of the PA active layer by imaging the isolated PA film. To isolate the PA thin film, a membrane coupon of ~1 cm × 1 cm in size was placed onto a silicon wafer and the PES substrate and foulant (if any) were dissolved by a few drops of DMF. The specimen was further washed with DMF and dried in a 40 °C vacuum oven. Prior to AFM imaging, multiple parallel dents were scratched on the isolated PA films using a needle without damaging the silicon wafer. The hard native silicon surface required only minimal care to prevent scratching of the substrate[43]. In practice, it is therefore easy to ensure that the silicon wafer was not damaged after scratching, and the absence of scratches can be confirmed during AFM test. The thickness of the PA thin film was then determined by scanning the border region between the PA film and the silicon wafer. AFM images were processed using Nanoscope Analysis software.

X-ray photoelectron spectroscopy (XPS, PHI 5000 C ESCA System) analyses and attenuated total reflection Fourier transform infrared spectroscopy (ATR-FTIR, Thermo Scientific Nicolet iS5) were conducted to investigate the surface composition of PA TFC membranes. The zeta potential of the membrane surface was evaluated by an electrokinetic analyzer (SurPASS 3, Anton Paar) for solid surface analysis at pH=7 and 10.

2.7 Nanofiltration performance test

A laboratory-scale cross-flow membrane filtration apparatus with an effective area of 9.1 cm^2 was used to test the nanofiltration performance of upcycled TFC PA membranes.[44] A 10 L DI

189 water sample was recirculated for 4 h for membrane precompaction at 7 bar with a cross-flow
190 velocity of 20.0 cm/s to stabilize the permeate flux. The feed solution temperature was kept
191 constant at 25.0 ± 0.5°C. The water flux and rejection rate of salts were measured at 6 bar. The
192 water flux (J_w), rejection of multiple salts (R) and water permeance were evaluated according
193 to the following procedures.

194 The water flux J_w is determined by Eq. (1).

195 $$J_w = \frac{\Delta w}{\rho A \Delta t} \quad (1)$$

196 where Δw is the weight change of permeate during filtration time Δt, A is the effective area of
197 each cross-flow cell, and ρ is the density of the permeate. The rejection of multiple salts (R)
198 was calculated based on the conductivity of the feed (C_f) and permeate (C_p) solutions (Eq. (2)).

199 $$R = (1 - \frac{C_p}{C_f}) \times 100\% \quad (2)$$

200 Water permeance refers to the water flux per unit applied pressure, as shown in Eq. (3),
201 where ΔP is the applied pressure for the cross-flow filtration experiment.

202 $$\text{Water permeance} = \frac{J_w}{\Delta P} \quad (3)$$

203 **2.8 Gold nanoparticle filtration tests**

204 GNPs are expected to closely follow streamlines and are useful markers for water transport
205 pathways.[31,45] Since both the GNP and membrane surface were negatively charged in this study,
206 the deposition of GNPs onto PA must be induced by the drag force. In the GNP filtration
207 experiment, equal volume of GNP solution was used for filtration through membranes, which
208 means that the final deposition amount of GNP on the membrane surface is equal. The only
209 difference of GNP deposition on the membrane surfaces is the uniformity which depends on
210 the water permeable sites on the membrane surfaces. Therefore, in this case, although the initial

water fluxes of various membranes are different, the distribution of GNP can effectively reflect the water permeable sites on the membrane surface.

GNP filtration tests were performed in a dead-end filtration Amicon cell (type 8050, effective area 13.4 cm^2) without stirring. The applied pressure for precompaction (using pure water for 30 min) was controlled at 5.0 bar, and the temperature was maintained at 25°C. Then, 40 mL of a dilute solution of GNPs in pure water (1.0×10^{12} particles/mL) was carefully added into the test cell for filtration experiments until 10 mL of the solution was left. All tested membranes were dried at 45°C for 3 h under vacuum before preparing samples for projected area TEM.

DMF was used to dissolve the PES substrate and foulants, and the PA film was carefully transferred onto copper grids. Projected area transmission electronic microscope (TEM) images were acquired with a TF20 TEM (FEI, USA) at an accelerating voltage of 200 kV.

3. Results & discussion

3.1 Microfiltration substrates fouled by different biopolymers

The biopolymer-fouled substrates were prepared by fouling PES microfiltration membranes via vacuum filtration of solutions of different biopolymers, including SA, BSA, HA and microbial EPS. The microbial EPS were used to represent the real fouling conditions induced by the combined effects of various biopolymer foulants, e.g., carbohydrates, proteins, and humic substances[28]. The impact of membrane fouling on the surface morphology and properties of PES microfiltration membrane was investigated, since it could significantly affect the formation of the PA active layer via IP and the properties of TFC PA membranes.[34,35] SA and BSA fouling, which was not obvious by visual observation (Figure 3A), could be revealed by SEM with a typical gel-like structure (Figure 3B and Figure S4). The lowest loading mass was observed for the BSA-fouled membrane (Figure 3C, 3.44 ± 0.35 μg/cm^2), which was ascribed to the relatively weak interaction between the functional groups of PES and BSA.[46,47] The weak

interaction, which may lead to delamination, can be neutralized by other adhesive foulants (e.g., SA) in the real membrane fouling conditions. The quantity of HA deposited on the membrane surface was the largest (17.61 ± 4.13 μg/cm^2) compared with those of BSA and SA, resulting in stacking of HA particles on the membrane surface as observed by SEM. For microbial EPS that are primarily composed of carbohydrates, proteins and humic substances (rather than the single component of SA, BSA and HA)[28], the fouling manner depends strongly on the dominant foulant component, which was protein (53.49%) in this case (Figure 3C). Therefore, a gel-like fouling structure was also observed for the EPS fouled substrate. The stability of biopolymer fouled substrates was evaluated by immersing membrane coupons into *n*-hexane (Figure S5), with results showing evidenced that the foulants on substrates were not removed during IP process.

The decrease in surface pore size (Figure 3B and Figure S6) for fouled substrates was inversely proportional to the increased loading mass. As expected, the pure water permeance (PWP) decreased significantly (p<0.05) for all fouled membranes (Figure 3D and Figure S7), especially for HA- and EPS-fouled membranes with a high foulant loading mass. Accompanied by fouling by HA or EPS solutions, the PWP through the HA- and EPS-fouled membranes decreased from ~10000 to ~1500 and ~2100 L m^{-2} h^{-1} bar^{-1}, respectively. Interestingly, although the PWPs of the HA- and EPS-fouled membranes were quite low compared with that of the control PES membrane and fell within the typical range of real fouled/end-of-life microfiltration membranes, they were still comparable with those of the UF membranes (typically 200-2000 L m^{-2} h^{-1} bar^{-1}) widely used as typical supports for forming TFC PA membranes[39].

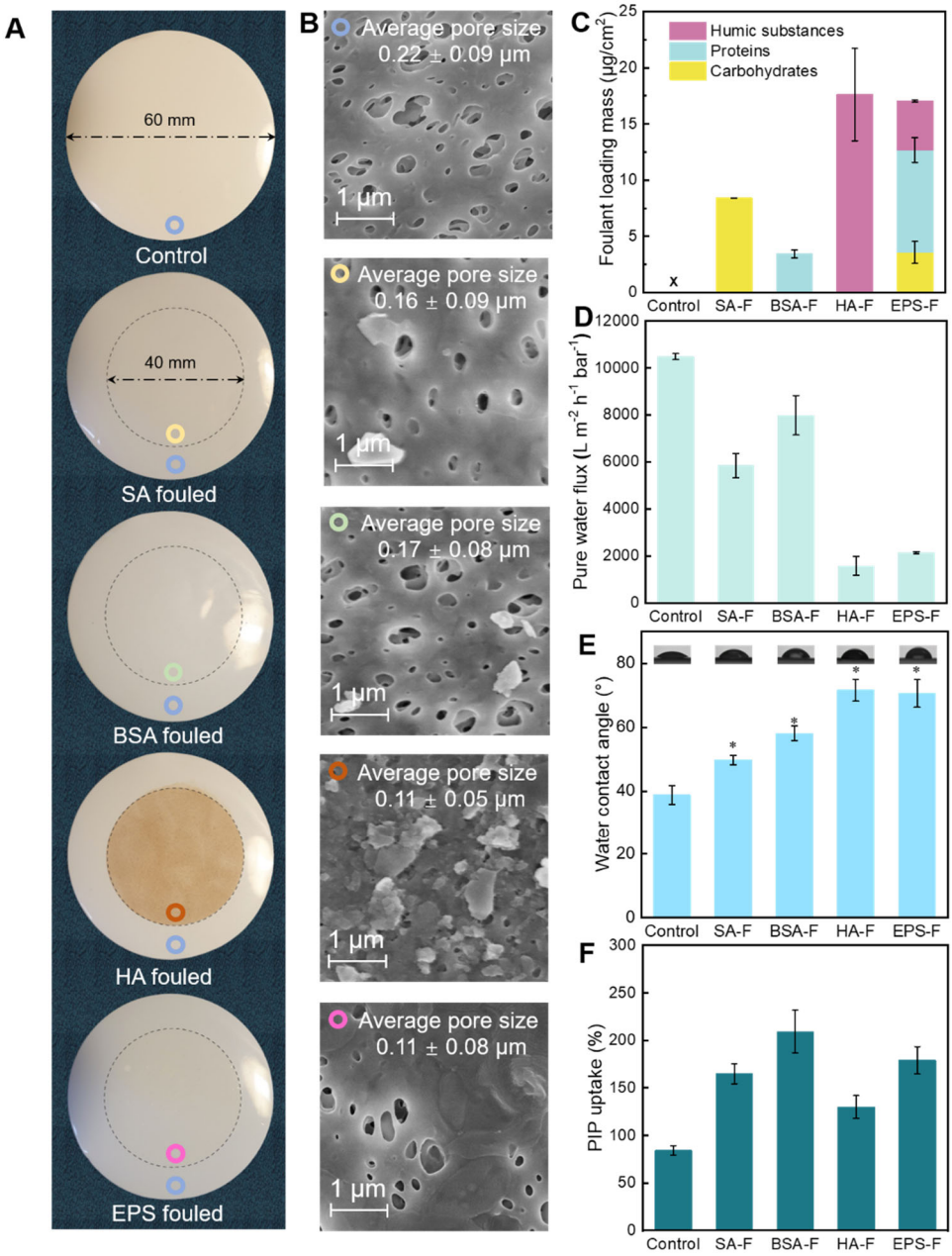

Figure 3. Characterization of the biopolymer fouled microfiltration substrates. (A) Photo of the biopolymer fouled substrates; (B) SEM images of the control and biopolymer fouled substrates; (C) Loading mass of foulants on the biopolymer fouled substrates; (D) Pure water permeance of microfiltration substrates before (control) and after biopolymer fouling, which was determined at pressure of 0.9 bar; (E) Water contact angle characterization of surfaces of different substrates; (F) PIP uptake by different substrates. The blue circle represents the clean

substrate, while the yellow, cyan, red and pink circles indicate the substrates fouled by SA, BSA, HA and EPS, respectively.

The change in surface properties by deposition of foulants was further supported by the larger water contact angles of the fouled membranes over that of the control PES substrate (Figure 3E), suggesting a change in surface energy (polarity). This change was attributed to both the narrowed surface pore size, the increased surface roughness (Figure S8) and the functional groups of biopolymers deposited. Based on the results of the water contact angle, pore density and pore size, we could conclude that the low water flux of the biopolymer fouled membranes was caused by combination of these factors. We further measured the PIP uptake capacities of the control and fouled membranes (Figure 3F), which governed the actual quantity of PIP for reaction and the diffusion rate of PIP into *n*-hexane[31]. The PIP uptake increased with the presence of biopolymer foulants on/in the membranes (Figure 3F). The pH of 0.05 wt/v % PIP/water is measured to be 9.7, at which -COOH and -OH of biopolymer foulants are fully and partially dissociated, respectively, presenting a negative charge. They can easily attract the PIP with positively charged >NH group (at pH=9.7) by electrostatic interaction. The foulants in real cases are typically abundant with various functional groups including the above negatively charged groups[19], which implies that the increased PIP uptake can also be achieved via electrostatic interaction or other forces[48,49]. The higher PIP uptake by biopolymers over PES substrates influenced the subsequent IP reaction due to the increased available monomer quantity and reduced diffusion rate of PIP, which resulted in formation of a more uniform, thinner and denser PA rejection layer[36].

3.2 Characterization of polyamide membranes upcycled from biopolymer fouled substrates

Typical IP processes were induced on the surface of the control and biopolymer fouled membranes via the reaction of PIP and TMC at the water-hexane interface. SEM

characterization of membranes after IP indicated the formation of ultrathin and smooth surfaces of PA for both control and upcycled NF membranes (Figure 4A and Figure S9). By comparison between cross-sectional SEM images of different substrates (Figure S4) and various TFC membranes (Figure S9), we concluded that the PA layer was formed on the substrates. The magnified SEM images (Figure S10) focusing on the pore-like structure further confirms that the PA layer covered and floated on the pores of the substrates. Despite the apparent difference in the surface properties of the substrate membranes, the roughness and water contact angle of the PA layer of the control and upcycled NF membranes were nearly identical (Figures 4B and C), even though the surface morphology underneath the PA layer of the NF membranes seemed to be different (Figures 3A and B). The average PA layer thicknesses of the NFcontrol, NF-SA, NF-BSA, NF-HA and NF-EPS, measured by an AFM probe (Figure S11 and 4D) [50], were 58 ± 2, 43 ± 2, 43 ± 4, 40 ± 2, and 46 ± 2 nm, respectively. The TFC membranes upcycled from fouled substrates had a thinner (p<0.05) PA layer than the membrane based on the control substrate. This suggested a decreased resistance to water transport, benefiting from the IP condition regulated by the biopolymer fouled substrates, which can be reflected by the previously observed changes of PIP uptake.

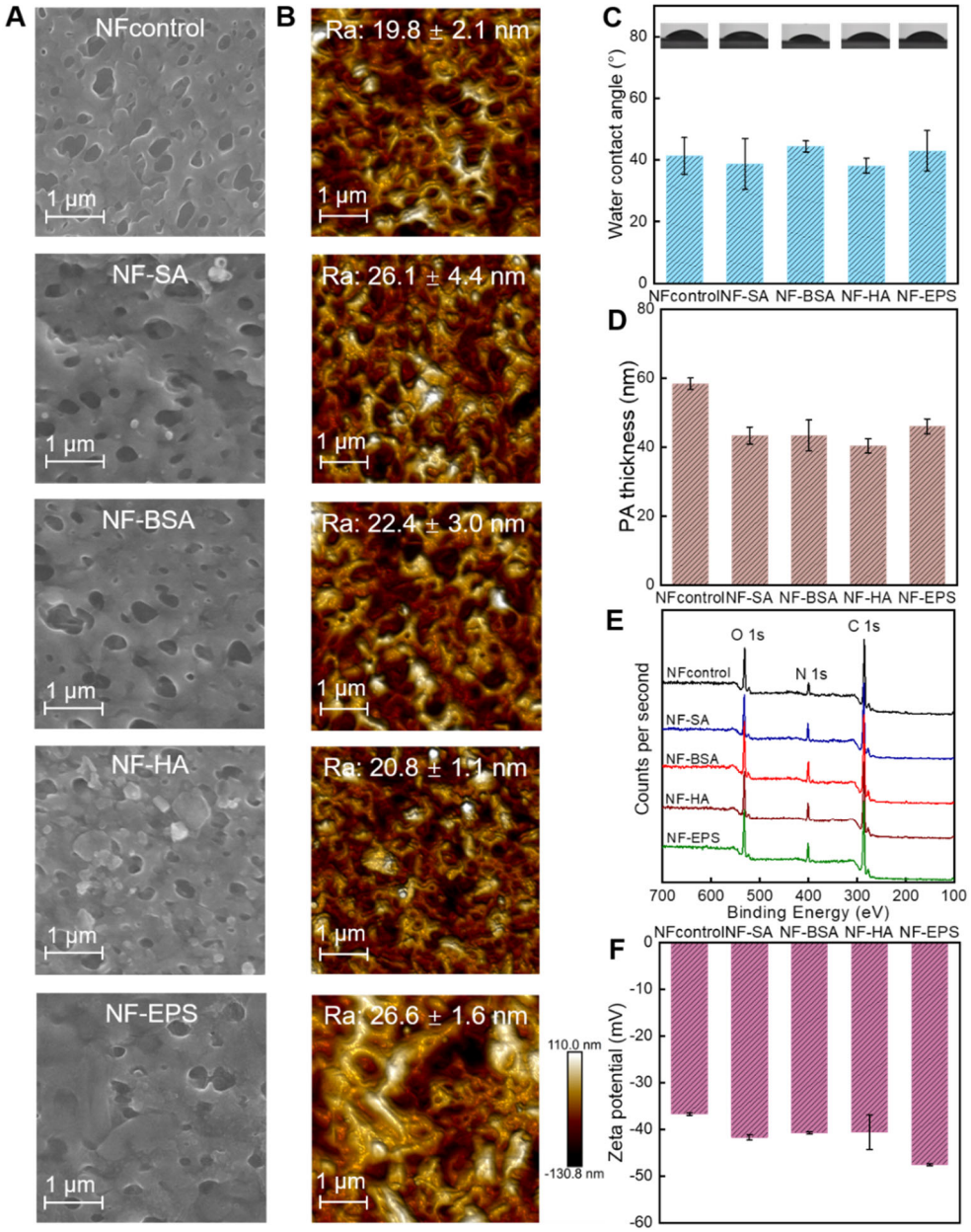

Figure 4. Characterizations of upcycled TFC PA membranes based on clean and biopolymer-fouled substrates. (A) SEM images that exhibit thin PA layer formation on different substrates; (B) AFM images of surfaces of TFC PA membranes, which were calibrated with a same color scale; (C) Water contact angle characterization of surfaces of TFC PA membranes; (D) PA thickness profile of different TFC membranes measured by AFM; (E) XPS survey spectra; (F) Surface zeta potential of TFC PA membranes.

312 The XPS spectra of the five PA active layers, one formed on the control substrate and the
313 others on the fouled substrates, suggested that they have the same chemical elements C, N, and
314 O as an indication of the PA chemistry (Figure 4E and Table S2). No S (characteristic element
315 of the PES substrate) was detected (the S2*p* peak is usually centered at approximately 154.0 eV)
316 in these spectra, confirming a defect-free PA layer covering on the membrane surfaces. To
317 quantify the chemical species within the structure, the O 1s and N 1s peaks of the XPS spectra
318 were deconvoluted (Figure S12), and the detailed information on the chemical compositions of
319 the PA active layer is summarized in Table 1. The core level O 1s spectrum demonstrated the
320 dominance of the amide bond at ~530.5 eV (N-C=O) and the presence of the remaining
321 unreacted acyl chloride groups on TMC which were eventually hydrolyzed into the carboxylic
322 acid group at ~532.5 eV (O-C=O). The core level N 1s spectrum also confirmed the amide bond
323 at ~399.5 eV (N-C=O) with a small contribution of unreacted imino group at ~398.0 eV (>NH).
324 The density of carboxylic acid groups and unreacted imino groups in the PA active layer
325 prepared on the fouled substrates was lower than that on the control substrate.
326 ATR-FTIR characterization (Figure S13) also confirmed the formation of amide group (C=O
327 stretching by amide I at 1658 cm^{-1}) in various membranes. The ATR-FTIR characterization can
328 detect functional groups (several hundreds of nm) deeper than XPS characterization (several
329 nm). Therefore, the amide group detected by ATR-FTIR can be attributed to the polyamide
330 layer and possibly amides reacted from carboxyl groups of the foulant molecules and imino
331 groups of PIP, which help stabilize the interaction between PA layer and foulant layers.
332
333 **Table 1.** Surface chemical components of polyamide NF membranes prepared from clean and
334 fouled substrates.

Samples	**O1s**	**N1s**

	Energy (eV)	Species	(%)	Energy (eV)	Species	(%)	Degree of network cross-linking (%)
NFcontrol	531.0	N-C=O	78.9	398.0	R>NH	10.0	12.1
	532.8	O-C=O	21.1	399.5	N-C=O	90.0	
NF-SA	530.7	N-C=O	86.3	397.5	R>NH	4.6	48.0
	532.6	O-C=O	13.7	399.5	N-C=O	95.4	
NF-BSA	530.5	N-C=O	83.8	398.0	R>NH	5.2	38.1
	532.3	O-C=O	16.2	399.7	N-C=O	94.8	
NF-HA	530.5	N-C=O	82.5	398.0	R>NH	8.1	28.1
	532.5	O-C=O	17.5	399.5	N-C=O	91.9	
NF-EPS	530.5	N-C=O	82.5	397.9	R>NH	8.8	24.3
	532.3	O-C=O	17.5	399.3	N-C=O	91.2	

Although the use of very diluted monomers (*i.e.*, 0.05 wt/v% PIP/water and 0.04 wt/v% TMC/*n*-hexane) resulted in a relatively low cross-linking degree for the control membrane (Table 1, 12.1%), the presence of foulants on the membrane surface substantially increased (p<0.05) the degree of cross-linking of the PA layer, e.g., 48.0% for the NF-SA membrane. This change was ascribed to the combined effect of optimization of the substrate surface properties and PIP uptake, which substantially affected the IP process[36,37].

To further understand the layered structure of upcycled PA membranes, etching and XPS analysis were performed for obtaining the XPS depth profile at the atomic level (Figure S14). The NF-SA membrane was selected as the model upcycled PA membrane. We observed a decrease in the intensity of O 1s and N 1s with an increase of etching depth from 0 nm to 380

nm, while the sulfur peak showed a gradual increase (Figure S14A). The trends are more clearly shown in the high-resolution O 1s spectra (Figure S14B), N 1s spectra (Figure S14C), and S 2p spectra (Figure S14D). Analysis on the atomic concentration (O, N, S) and its differential with depth further indicated a triple-layered structure for the NF-SA membrane (Figure S15). Furthermore, the nitrogen can be detected even at foulant layer and skin of PES substrate, which suggest a possible anchorage of PA layer into foulant layer and pores of PES substrates. This ensures the structural strength of upcycled PA membranes.

The upcycled NF membranes showed a more negatively charged surface than the NFcontrol (Figure 4F), not in accordance with the tendency of the results for the cross-linking degrees (Table 1). This can be explained by the fact that the biopolymer foulants underneath the PA layer are also negatively charged at pH = 7, possibly contributing to an increased overall net negative charge. This means that the biopolymer foulant interlayer may also contribute, in the aspect of Donnan exclusion, to the transport properties of the whole NF membrane, which is beneficial for the rejection of divalent or multivalent ions.[51]

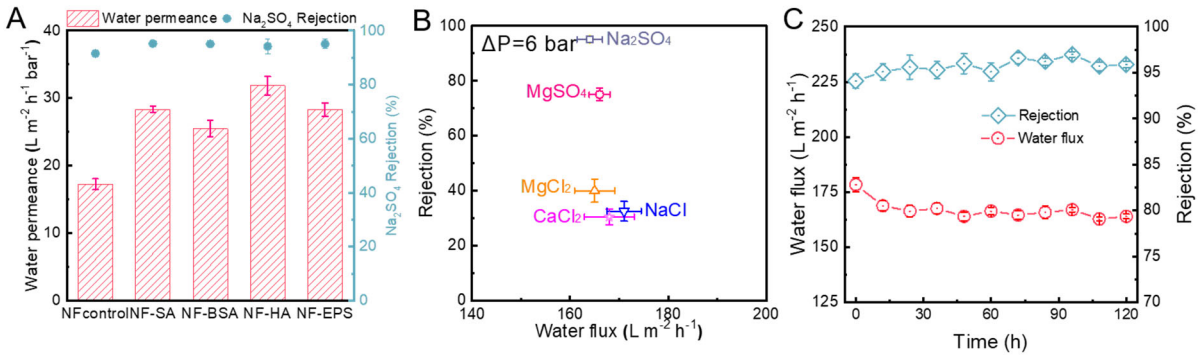

Figure 5. NF performance of the control and upcycled TFC PA membranes. (A) Water permeance and Na_2SO_4 rejection (salt concentration: 10 mM; applied pressure: 6 bar); (B) Water flux and rejection of the NF-EPS membrane with respect to different salt solutions (salt

concentration: 10 mM; applied pressure: 6 bar); (C) Variation of flux and rejection of the NF-EPS membrane as a function of time (Na_2SO_4 concentration: 10 mM; applied pressure: 6 bar).

3.3 Efficient nanofiltration of upcycled TFC PA membranes

The NF performance of control and upcycled TFC PA membranes was tested in a laboratory cross-filtration system. Surprisingly, the upcycled PA TFC membrane exhibited higher ($p<0.05$) water fluxes and Na_2SO_4 rejection rates than the membrane based on a control substrate (Figure 5A), in contrast to the decreased PWP of substrates with biopolymer fouling (Figure 3E). Specifically, the NF-HA membrane showed the highest water permeance of 31.9 ± 1.4 L m^{-2} h^{-1} bar^{-1}, which was approximately 2.0 times that of the NFcontrol membrane, even though the HA-fouled substrate had 85% decrease in PWP compared with that of the control substrate. The Na_2SO_4 rejection rate of the HA-NF membrane (~94%) was also higher than that of the NFcontrol membrane (~91%). The NF-EPS membrane, as a practical verification case, also had improved water permeance (28.3 ± 1.0 L m^{-2} h^{-1} bar^{-1}) and Na_2SO_4 rejection (~95%). Combined with the improved NF performance of upcycled membranes based on SA-, BSA-, HA-fouled substrates, we can confirm the important roles of carbohydrates, proteins and humic substances in membrane formation and associated performance for NF-EPS membrane. These results evidently show that even fouled/end-of-life membranes with deteriorated water flux could be upcycled as substrates for fabricating high permeance PA TFC membranes.

The filtration performance of the NF-EPS membrane was evaluated for rejecting other salts (Figure 5B). While the NF-EPS membrane exhibited nearly similar permeating fluxes for all salts tested, the salt rejection rates for Na_2SO_4 and $MgSO_4$ were much higher than those for $MgCl_2$, $CaCl_2$ and NaCl due to the synergistic effect of strong Donnan exclusion and size sieving with the sulfate salts. We further evaluated the stability of the NF-EPS membrane

during a long-term cross-filtration test. In experiments with 10 mM Na_2SO_4 feed solution and an applied pressure of 6 bar, no appreciable change in the permeating flux and salt rejection was observed after membrane compaction in continuous cross-filtration up to 120 h (Figure 5C).

3.4 Mechanistic insights

The improved Na_2SO_4 rejection rate of the TFC membranes based on fouled substrates should be mainly attributed to the increased cross-linking degree (narrowed pore size) and surface net negative charge (Figure 4F and Table 1). The larger pores and much higher permeance of the MF substrates compared to conventionally utilized UF membrane was one of the origins of the high permeance of prepared NF membranes. Moreover, for the increased water permeance of upcycled membranes over that of NFcontrol, the thinner PA layers formed on the biopolymer-fouled substrates could be another reason. We further hypothesized that the biopolymer foulants might also benefit the water transport through membranes by other mechanisms, *e.g.*, possibly via providing additional channels for water transport.

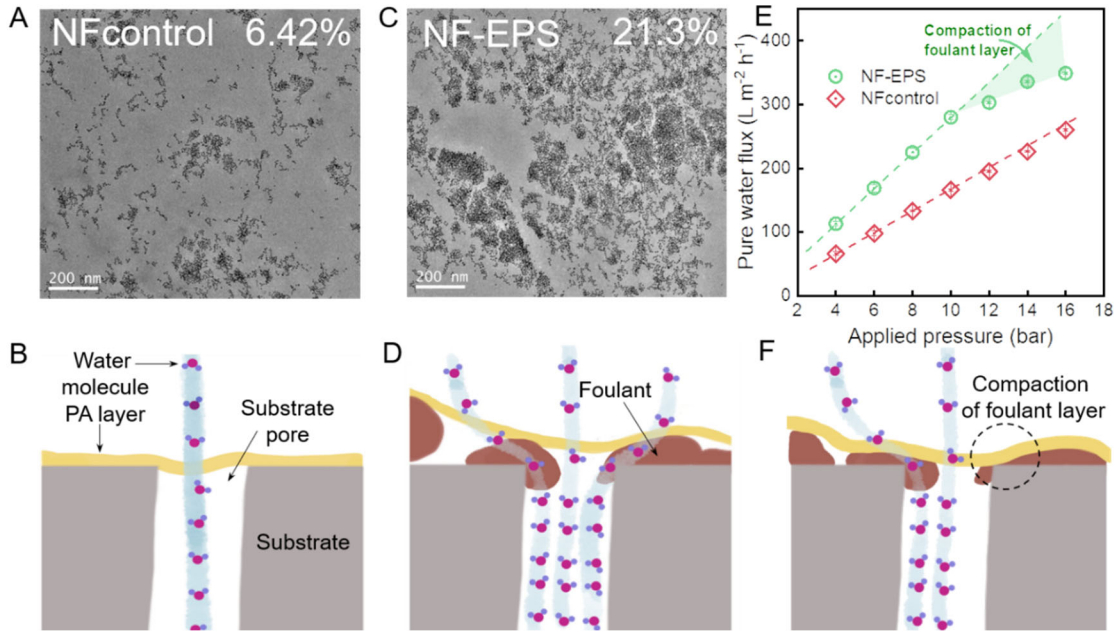

Figure 6. Mechanistic insights into the enhanced NF performance of the upcycled TFC PA membranes. (A, C) Projected area TEM images showing GNP deposition on the surfaces of the NFcontrol and NF-EPS membranes after filtration tests (1.0×10^{12} particles ml^{-1}, 25 °C, 5.0 bar), GNP percent surface area coverage is given in the upper right corner of each image; (E) Water flux of NFcontrol and NF-EPS membranes as a function of applied pressure; (B, D, F) Schematics of the water transport through PA layer of a clean substrate-based, an upcycled TFC and a compacted upcycled TFC membranes.

To verify this hypothesis, we adopted GNPs as probes in combination with TEM to visualize the spatial distribution of sites for water permeation in the PA layers of NFcontrol and NF-EPS (Figs. 6A and C). GNPs are expected to closely follow streamlines and are useful markers for water transport pathways [31,45]. Since both the GNP and membrane surface were negatively charged in this study, the deposition of GNPs onto PA must be induced by the drag force. Projected area TEM micrographs suggested that the deposition of GNPs was not uniform across the PA surface for both membranes. Nevertheless, the deposition of GNPs on the surface of the NF-EPS membrane was significantly different (more uniform, $p<0.05$) from that on the NFcontrol (Figures 6A and C, Figure S16). This provides visual evidence supporting the enhanced uniformity of water permeable sites and hence increased water transport channels in the PA layer of the upcycled NF membrane. The additional channels created by biopolymer foulants facilitated water transport from the PA film formed on the nonporous domain of the PES substrate to neighboring pores (Figure 6B and D). The effective area of the PA active layer for water transport was therefore increased due to the mediation by the foulant. Further, we confirmed that the surface foulants contributed positively to the improved water flux compared to the inner foulants (Figure S17).

We then tested the pure water flux of NFcontrol and NF-EPS membranes as a function of applied pressure (Figure 6E). The water flux of NFcontrol increased linearly with the applied pressure, and similar trend was observed for NF-EPS membrane within the pressure range of 4-10 bar. However, the increase rate of water flux of NF-EPS membrane decreased apparently as applied pressure exceeded 12 bar, inducing a green region in Figure 6E, which should be ascribed to the compaction of foulant layer by high pressure[52,53]. The compaction effect was further visually evidenced by SEM characterizations (Figure S18). These results further confirmed the mediation role of foulants (Figure 6F). The compaction can stabilize the composite structure of upcycled membranes, and the interaction between the polyamide layer and the foulant layer (mainly involves van der Waals force, π-π conjugation and possible covalent bonds) also help ensure the interlayer adhesion. The compaction effect also implies that the rigidity of foulants should be considered in the future fabrication of upcycled TFC PA membrane.

3.5 In-situ formation of the upcycled PA TFC membrane.

To further highlight the feasibility of upcycling biopolymer-fouled MF membranes, in-situ formation of the upcycled PA TFC membranes was carried out in a laboratory cross-flow cell (Figures 7A, B). The cross-flow cell containing substrate/membrane was not deconstructed during entire fouling and IP process, only with change of pipeline connections. The SEM characterizations (Figure 7C, D) indicated that the membrane surface for in-situ (online) prepared NF-EPS showed no significant difference compared with the NF-EPS prepared in typical offline IP process. The separation properties of in-situ NFcontrol and NF-EPS membranes were evaluated in terms of water permeance and Na_2SO_4 rejection (Figure 7E). The in-situ NF-EPS membrane showed a water permeance of 24 L m^{-2} h^{-1} bar^{-1} and a 97% rejection for Na_2SO_4, which was also higher than those of in-situ NFcontrol (13 L $m^{-2}h^{-1}bar^{-1}$ and a 94%

453 Na_2SO_4 rejection). In contrast to the membranes fabricated using typical offline IP process
454 (Figure 5A), the slightly lower water permeance and higher Na_2SO_4 rejection for in-situ formed
455 NFcontrol and NF-EPS membranes can be ascribed to the changed IP conditions. Nevertheless,
456 this result well demonstrates the practical feasibility of upcycling biopolymer-fouled substrates
457 to fabricate high-permeance TFC PA membranes.

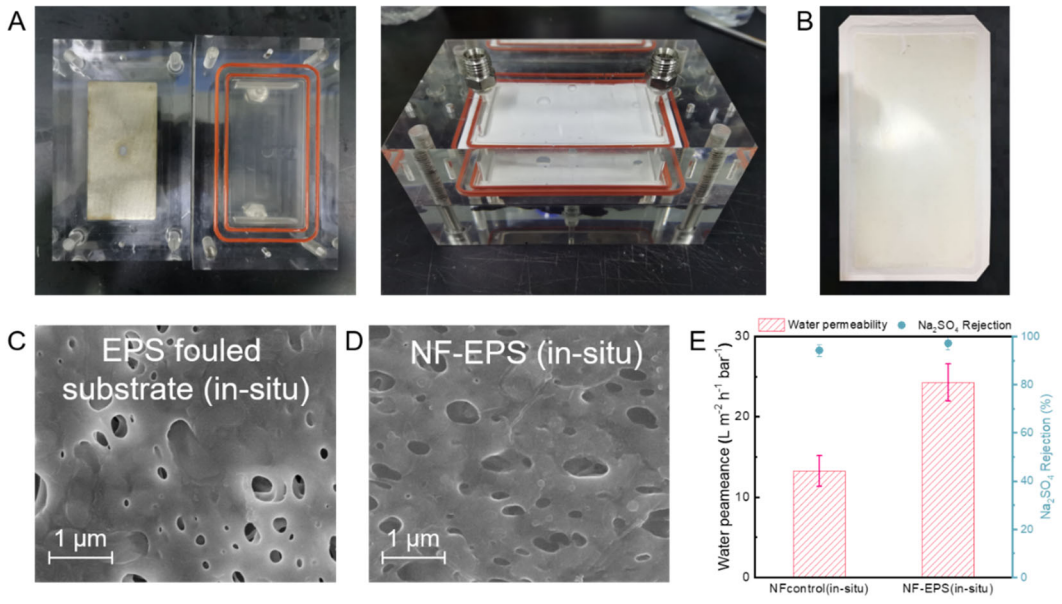

458

459 **Figure 7.** In-situ formation of the PA TFC membrane upcycled from clean or EPS fouled
460 substrates in a cross-flow cell. (A) Cross-flow cell used for in-situ formation of upcycled PA
461 TFC membranes; (B) Photo of the in-situ EPS fouled substrate; (C) SEM image of the in-situ
462 EPS fouled substrate; (D) SEM image of in-situ formed NF-EPS membrane; (E) Water
463 permeance and Na_2SO_4 rejection of in-situ formed NFcontrol and NF-EPS membranes (salt
464 concentration: 10 mM; applied pressure: 6 bar).

465

466 **3.6 Upcycling real fouled MF substrates to obtain PA TFC membranes.**

467 We further evaluated the feasibility of forming PA layer on the real fouled MF substrates.
468 Fouled PVDF MF membranes from an engineered MBR were gently washed by water (Figures
469 S19A and S19B) and directly used for interfacial polymerization. Although the real fouled

substrate possessed a significant different morphology and foulant composition (Figure 8A) compared with the artificially fouled substrates (such as SA-F, BSA-F and HA-F), a uniform and continuous PA layer could also be formed on the surface of real foulant layer, which was confirmed by SEM and XPS analyses (Figures 8A, 8B, S20 and S21). The nanofiltration performance test (Figure 8C) indicated that Na_2SO_4 rejection rate of the real upcycled membrane was lower than those of membranes upcycled from artificially fouled substrates at the same monomer concentration (0.05 wt/v% PIP/water and 0.04 wt/v% TMC/*n*-hexane). Fortunately, the Na_2SO_4 rejection of the real upcycled membranes could be improved by increasing monomer concentrations, suggesting the flexibility of the upcycling strategy. Moreover, introducing green solvent into membrane preparation can allow a more sustainable membrane fabrication procedure[54–56]. Therefore, to modify the strategy based on green chemistry perspective, we further investigated the feasibility of replacing *n*-hexane by a greener alternative, *n*-heptane, and the results demonstrated that TFC PA membranes with favorable nanofiltration performance could also be fabricated based on *n*-heptane solvents.

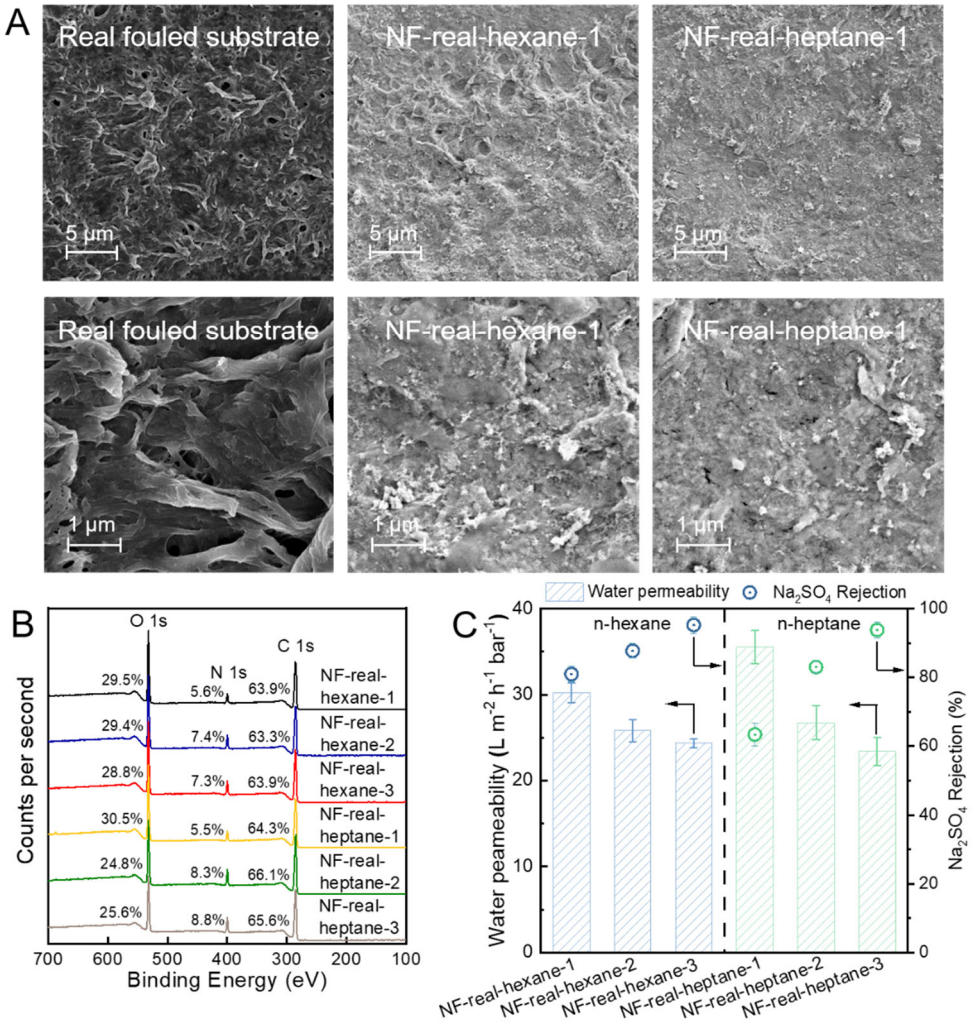

Figure 8. PA layer formation on real fouled MF substrates. (A) SEM image of the real fouled substrate and corresponding upcycled membranes; (B) XPS spectra of various TFC PA membranes upcycled from real fouled substrates; (C) Water permeance and Na_2SO_4 rejection of various TFC PA membranes upcycled from real fouled substrates (salt concentration: 10 mM; applied pressure: 6 bar).

3.7 A closed eco-loop of membrane material recycling and environmental implications.

The strategy to downcycle end-of-life RO/NF membranes as candidates to correspondingly prepare NF/UF membranes has been gradually validated to be practical from both economic and waste recycling views. In our work, the high-pressure TFC membrane upcycled from a

fouled/end-of-life microfiltration substrate is also feasible and beneficial for forming a closed eco-loop of membrane material recycling. Ideally, in the closed eco-loop, high-pressure/low-pressure membranes after use can be correspondingly downcycled/upcycled to form new low-pressure/high-pressure membranes, which can be recycled again after another round of use. The closed eco-loop can not only effectively decrease the amount of abandoned end-of-life membranes and reduce the negative environmental impact of their disposal but also grant us the opportunity to fabricate high-performance TFC membranes in a cost-effective and environmentally friendly way. The actual life span of either low-pressure or high-pressure membranes is hence prolonged in the closed eco-loop of membrane material recycling, thus significantly decreasing their environmental footprint. Nevertheless, considering the various chemical components, thickness, adhesion and morphology of different foulants on MF substrates in real conditions, the IP process needs to be optimized/customized to guarantee its effectiveness for forming uniform and continuous PA layer.

In practice, the materials used for constructing the module housings, flow spacers, and interconnects are equivalent to, or even greater, in mass than the membranes themselves, and it would arouse economic concerns if the upcycling process were implemented after disassembling MF/UF modules. Therefore, the upcycling of fouled/end-of-life membranes should be completed with the membranes remaining in their modules. The *in-situ* formation of the upcycled TFC NF membrane based on biopolymer-fouled substrate has been demonstrated here in a lab-scale cross-flow cell. Nevertheless, this *in-situ* IP process needs to be further validated for membrane modules, for example, combining the IP process with traditional membrane cleaning procedure[57], or possibly using concentration polarization enhanced modification technique[58,59]. In addition, *in-situ* upcycling of fouled/end-of-life hollow fiber membrane modules is of great interest in the future due to the high consistency in configurations between low-pressure and high-pressure hollow fiber membrane modules.

4. Conclusions

Directly fabricated on microfiltration substrates fouled by biopolymers, TFC membranes with cross-linked, defect-free, and ultrathin PA active layers demonstrated superior potential in high-performance nanofiltration. The foulants on the substrate manipulate the surface properties, PIP uptake and IP process, and subsequently regulate the structure of the formed PA layer. In contrast to the decreased PWP of substrates with biopolymer fouling, the upcycled NF membrane exhibited excellent water flux (~30 L m^{-2} h^{-1} bar^{-1}) and Na_2SO_4 rejection rate (~95%). The foulants between the PA layer and substrate can construct additional channels for water transport. The PA layer formation could also be achieved on real fouled MF substrates. These prove the concept that even fouled substrates can be a favorable platform for interfacial polymerization. This proof-of-concept study also paves the way for upcycling fouled/end-of-life low-pressure membranes to fabricate new high-pressure membranes for water purification, forming a closed eco-loop of membrane recycling.

Electronic Supplementary Information

†Electronic Supplementary Information (ESI) available: Information on materials, experimental procedure and additional membrane characterizations. See DOI: 10.1039/x0xx00000x

Conflicts of interest

There are no conflicts to declare.

Acknowledgements

We thank the National Natural Science Foundation of China (grants 51838009 & 51925806), and the Peak Discipline Construction Program in Environment and Ecology of Shanghai for the financial support of the work.

References

1 H. B. Park, J. Kamcev, L. M. Robeson, M. Elimelech and B. D. Freeman, *Science*, 2017, **356**, eaab0530.
2 M. Elimelech and W. A. Phillip, *Science*, 2011, **333**, 712–717.
3 C. Y. Tang, Z. Yang, H. Guo, J. J. Wen, L. D. Nghiem and E. Cornelissen, *Environmental Science & Technology*, 2018, **52**, 10215–10223.
4 H. Fröhlich, L. Villian, D. Melzner and J. Strube, *Chemie Ingenieur Technik*, 2012, **84**, 905–917.
5 A. Cassano, C. Conidi and E. Drioli, in *Intensification of Biobased Processes*, 2018, pp. 397–429.
6 E. Coutinho de Paula and M. C. Santos Amaral, *Journal of Cleaner Production*, 2018, **194**, 85–93.
7 J. Landaburu-Aguirre, R. García-Pacheco, S. Molina, L. Rodríguez-Sáez, J. Rabadán and E. García-Calvo, *Desalination*, 2016, **393**, 16–30.
8 W. S. Ang, A. Tiraferri, K. L. Chen and M. Elimelech, *Journal of Membrane Science*, 2011, **376**, 196–206.
9 W. Lawler, Z. Bradford-Hartke, M. J. Cran, M. Duke, G. Leslie, B. P. Ladewig and P. Le-Clech, *Desalination*, 2012, **299**, 103–112.
10 R. W. Baker, *Membrane technology and applications*, John Wiley & Sons, Chichester, West Sussex ; Hoboken, 3rd ed., 2012.
11 A. Lejarazu-Larrañaga, S. Molina, J. M. Ortiz, R. Navarro and E. García-Calvo, *Journal of Membrane Science*, 2020, **593**, 117423.
12 H. A. Le Phuong, N. A. Izzati Ayob, C. F. Blanford, N. F. Mohammad Rawi and G. Szekely, *ACS Sustainable Chem. Eng.*, 2019, **7**, 11885–11893.
13 M. I. Baig, E. N. Durmaz, J. D. Willott and W. M. de Vos, *Advanced Functional Materials*, **n/a**, 1907344.
14 B. A. Pulido, O. S. Habboub, S. L. Aristizabal, G. Szekely and S. P. Nunes, *ACS Appl. Polym. Mater.*, 2019, **1**, 2379–2387.
15 F. Fei, H. A. Le Phuong, C. F. Blanford and G. Szekely, *ACS Appl. Polym. Mater.*, 2019, **1**, 452–460.
16 G. Zhao, Y. Chen, X.-F. Li, S. Zhang and Y. Situ, *Green Chem.*, 2020, **22**, 2426–2433.
17 R. García-Pacheco, J. Landaburu-Aguirre, S. Molina, L. Rodríguez-Sáez, S. B. Teli and E. García-Calvo, *Journal of Membrane Science*, 2015, **495**, 305–315.
18 M. R. Moradi, A. Pihlajamäki, M. Hesampour, J. Ahlgren and M. Mänttäri, *Journal of Membrane Science*, 2019, **584**, 300–308.
19 W. Guo, H.-H. Ngo and J. Li, *Bioresource Technology*, 2012, **122**, 27–34.
20 K. Kimura and Y. Oki, *Water Research*, 2017, **115**, 172–179.
21 K. Kimura, K. Tanaka and Y. Watanabe, *Water Research*, 2014, **49**, 434–443.
22 C. J. Gabelich, T. I. Yun, K. P. Ishida, M. B. Leddy and J. Safarik, *Desalination*, 2004, **161**, 263–276.
23 Z. Wang, Z. Wu and S. Tang, *Water Research*, 2009, **43**, 2504–2512.
24 N. R. Maddela, Z. Zhou, Z. Yu, S. Zhao and F. Meng, *Appl. Environ. Microbiol.*, , DOI:10.1128/AEM.00756-18.
25 R. van Reis and A. Zydney, *Journal of Membrane Science*, 2007, **297**, 16–50.
26 H. Li and V. Chen, in *Membrane Technology*, eds. Z. F. Cui and H. S. Muralidhara, Butterworth-Heinemann, Oxford, 2010, pp. 213–254.

27 S. Gao, Y. Zhu, J. Wang, F. Zhang, J. Li and J. Jin, *Advanced Functional Materials*, 2018, **28**, 1801944.
28 Y.-F. Guan, B.-C. Huang, C. Qian, L.-F. Wang and H.-Q. Yu, *Water Research*, 2017, **113**, 89–96.
29 F. Galiano, K. Briceño, T. Marino, A. Molino, K. V. Christensen and A. Figoli, *Journal of Membrane Science*, 2018, **564**, 562–586.
30 D. Hou, T. Li, X. Chen, S. He, J. Dai, S. A. Mofid, D. Hou, A. Iddya, D. Jassby, R. Yang, L. Hu and Z. J. Ren, *Science Advances*, 2019, **5**, eaaw3203.
31 Z. Tan, S. Chen, X. Peng, L. Zhang and C. Gao, *Science*, 2018, **360**, 518–521.
32 M. R. Chowdhury, J. Steffes, B. D. Huey and J. R. McCutcheon, *Science*, 2018, **361**, 682–686.
33 S. Karan, Z. Jiang and A. G. Livingston, *Science*, 2015, **348**, 1347–1351.
34 Z. Wang, Z. Wang, S. Lin, H. Jin, S. Gao, Y. Zhu and J. Jin, *Nature Communications*, 2018, **9**, 2004.
35 A. K. Ghosh and E. M. V. Hoek, *Journal of Membrane Science*, 2009, **336**, 140–148.
36 Z. Yang, Z. Zhou, H. Guo, Z. Yao, X. Ma, X. Song, S.-P. Feng and C. Y. Tang, *Environmental Science & Technology*, 2018, **52**, 9341–9349.
37 X. Yang, Y. Du, X. Zhang, A. He and Z.-K. Xu, *Langmuir*, 2017, **33**, 2318–2324.
38 Y. Zhu, W. Xie, S. Gao, F. Zhang, W. Zhang, Z. Liu and J. Jin, *Small*, 2016, **12**, 5034–5041.
39 G. Gong, P. Wang, Z. Zhou and Y. Hu, *ACS Applied Materials & Interfaces*, 2019, **11**, 7349–7356.
40 H. Choi, A. A. Shah, S.-E. Nam, Y.-I. Park and H. Park, *Desalination*, 2019, **449**, 41–49.
41 W. Zhao, H. Liu, Y. Liu, M. Jian, L. Gao, H. Wang and X. Zhang, *ACS Appl. Mater. Interfaces*, 2018, **10**, 34464–34474.
42 B. Frølund, R. Palmgren, K. Keiding and P. H. Nielsen, *Water Research*, 1996, **30**, 1749–1758.
43 V. Freger, *Environ. Sci. Technol.*, 2004, **38**, 3168–3175.
44 R. Dai, H. Guo, C. Y. Tang, M. Chen, J. Li and Z. Wang, *Environ. Sci. Technol.*, 2019, **53**, 13776–13783.
45 F. A. Pacheco, I. Pinnau, M. Reinhard and J. O. Leckie, *Journal of Membrane Science*, 2010, **358**, 51–59.
46 D. T. Myat, M. B. Stewart, M. Mergen, O. Zhao, J. D. Orbell and S. Gray, *Water Research*, 2014, **48**, 108–118.
47 Y. Sun, K. Zhu, B. Khan, X. Du, L. Hou, S. Zhao, P. Li, S. Liu, P. Song, H. Zhang, S. Jiang, Z. Wang and S. Zha, *IOP Conf. Ser.: Mater. Sci. Eng.*, 2018, **301**, 012031.
48 Z. Yang, P.-F. Sun, X. Li, B. Gan, L. Wang, X. Song, H.-D. Park and C. Y. Tang, *Environ. Sci. Technol.*, , DOI:10.1021/acs.est.0c05377.
49 R. Dai, J. Li and Z. Wang, *Advances in Colloid and Interface Science*, 2020, **282**, 102204.
50 C. Boo, Y. Wang, I. Zucker, Y. Choo, C. O. Osuji and M. Elimelech, *Environmental Science & Technology*, 2018, **52**, 7279–7288.
51 W. R. Bowen and J. S. Welfoot, *Chemical Engineering Science*, 2002, **57**, 1121–1137.
52 M. T. M. Pendergast, J. M. Nygaard, A. K. Ghosh and E. M. V. Hoek, *Desalination*, 2010, **261**, 255–263.
53 M. Aghajani, M. Wang, L. M. Cox, J. P. Killgore, A. R. Greenberg and Y. Ding, *Journal of Membrane Science*, 2018, **567**, 49–57.
54 T. Marino, F. Galiano, A. Molino and A. Figoli, *Journal of Membrane Science*, 2019, **580**, 224–234.
55 L. Cseri and G. Szekely, *Green Chem.*, 2019, **21**, 4178–4188.
56 F. Russo, F. Galiano, F. Pedace, F. Aricò and A. Figoli, *ACS Sustainable Chem. Eng.*, 2020, **8**, 659–668.
57 Z. Wang, J. Ma, C. Y. Tang, K. Kimura, Q. Wang and X. Han, *Journal of Membrane Science*, 2014, **468**, 276–307.
58 R. Bernstein, S. Belfer and V. Freger, *Journal of Membrane Science*, 2012, **405–406**, 79–84.
59 R. Bernstein, S. Belfer and V. Freger, *Environ. Sci. Technol.*, 2011, **45**, 5973–5980.